Simulation of Pandemics in Real-cities: Enhanced and Accurate Digital-labs

Alessio Alexiadis, Andrea Albano, Amin Rahmat, Mehmet Yildiz, Adnan Kefal, Murat Özbulut, Nadi Bakirci, Diego Alexander Garzon Alvarado, Carlos Alberto Duque-Daza, Javier Hernando Eslava-Schmalbach

Simulation of Pandemics in Real-cities: Enhanced and Accurate Digital-labs

Alessio Alexiadis[a], Andrea Albano[a], Amin Rahmat[a], Mehmet Yildiz[b], Adnan Kefal[b], Murat Özbulut[c], Nadi Bakirci[d], Diego Alexander Garzon Alvarado[e], Carlos Alberto Duque-Daza[a,e], Javier Hernando Eslava-Schmalbach[f]

[a] School of Chemical Engineering, University of Birmingham, Edgbaston Birmingham B15 2TT, United Kingdom
[b] Faculty of Engineering and Natural Sciences, Sabanci University, 34956 Tuzla, Istanbul, Turkey
[c] Faculty of Engineering, Piri Reis University, 34940 Istanbul, Turkey
[d] School of Medicine, Acibadem University, İçerenköy, Kayışdağı 32, 34684 İstanbul, Turkey
[e] Department of Mechanical and Mechatronic Engineering, Universidad Nacional de Colombia, Cra 30 No 45-03. Bogotá, Colombia
[f] School of Medicine, Universidad Nacional de Colombia; Hospital Universitario Nacional de Colombia, Cra 30 No 45-03. Bogotá, Colombia

Abstract

This study develops a modelling framework for simulating the spread of infectious diseases within real cities. Digital copies of Birmingham (UK) and Bogotá (Colombia) are generated reproducing their urban environment, infrastructure, and population. The digital inhabitants have the same statistical features of the real population. Their motion is a combination of predictable trips (commute to work, school etc.), and random walks (shopping, leisure etc.). Millions of individuals, their encounters, and the spread of the disease are simulated by means of High Performance Computing and Massively Parallel Algorithms, for several months and a time resolution of 1 minute. Simulations accurately reproduce the covid-19 data for Birmingham and Bogotá both before and during the lockdown. The model has only one adjustable parameter calculable in early stages of the pandemic. Policymakers can use our digital cities as virtual labs for testing, predicting, and comparing the effects of policies aimed at containing epidemics.

1. Introduction

The epidemiological models used to predict the spread of infectious diseases are similar to the mathematical models used in chemistry. It is not a coincidence. They both describe the dynamics of populations evolving under the Law of Masses Action (LMA). The underlying principle is that of 'encounters between members' producing an effect on the population. This effect can be a chemical reaction in a population of molecules, or contagion in a population of humans. When population models are coupled with physical concepts like flux and conservation, they become compartmental model. Classical epidemiological models are compartmental models with the flux being computed from the LMA.

The appeal of compartmental models lies in their simplicity. The complex dynamics of large numbers of molecules or individuals is condensed into few ordinary differential equations. However, this simplicity comes at a cost. Standard epidemiological models do not account for space, behavioural aspects of the population or other external variables. These are introduced as case-specific adjustable coefficients that must be derived from data, making the model reliant on the timely availability of data. Moreover, every time the populations' behaviour changes due to lockdown or

other policies, these coefficients must be refitted to new data that will become available only *after* the policy is implemented.

To overcome the limitations of compartmental models, chemistry has moved beyond the LMA. Utilizing supercomputers, computational chemists today routinely simulate the trajectory and the collision of millions of atoms. This technique is called Molecular Dynamics (MD), and it is an irreplaceable tool in modern chemistry. Computational epidemiology, however, has not found its MD-equivalent yet.

This study proposes a granular approach for modelling the spread of infectious diseases in real cities. Millions of individuals, their encounters and contagion are simulated at the individual level. We named this approach Discrete Epidemiology (DE) for its mathematical similarity with MD, Discrete Multiphysics (e.g. Alexiadis 2015) and, in general, particle methods.

Methodologically, DE results in a technique that combines, within an efficient computational framework, several approaches used in epidemiology. As compartmental models, DE divides the population in compartments, and, like stochastic models, it represents contagion as a Monte Carlo process. Similarly to Census-Calibrate models (Zachreson et al. 2018; Fair et al. 2019), it generates a digital population that, like in Agent-Based Models (Cliff et al. 2020; Gomez et al. 2020), moves in a virtual city based on individual mobility plans. Also, like in human mobility models (Rhee et al. 2011), it accounts for the unpredictability of human behaviour overlaying a time-dependant Wiener (or Lévy) walk on top of the mobility plan. DE is computationally very efficient because it takes advantage of algorithms, such as Verlet lists and massive parallelization, developed in over 70 years of MD. Today, MD can simulate billions (Kadau et al. 2006), and even trillions (Tchipev et al. 2019), of atoms. This implies that, provided the right amount of time and resources, DE can potentially simulate the mobility of the entire human population.

The paper is organized as follows: initially, we present several 'toy models'. These introduce DE's theory step-by-step and, at the same time, validate the method against traditional epidemiological models. Each section introduces a new feature and is self-contained, meaning that it has its own independent 'Methods', 'Results' and 'Discussion'. Finally, all toy models are combined to simulate real cities with millions of inhabitants. We recreate digital versions of Birmingham in the UK (~1 million people) and Bogotá in Colombia (~10 million people) replicating their geography and infrastructure (city limits, countryside, trains, bus lines, stations etc.). Their virtual inhabitants have features coming from the statistics of the real population and relevant to their mobility and susceptibility to the disease (age, residence, household size, employment, workplace, commuting, distance of contagion, infection probability etc.). Once the digital city and its virtual population are generated, DE utilizes advanced hardware (high-performance and high-throughput computing) and software (massively parallel processing) to simulate the behaviour of all inhabitants in the city for several months. The position of every individual is updated every 60 seconds and when an infected individual encounters a susceptible one, the probability of infection is handled stochastically. These computer-generated cities are then used as virtual labs to understand the unique features of the city determining the evolution of the disease within its boundaries, and for testing the effect of policies aimed at containing its spread.

2. A first, simple, discrete model

Individuals are represented by particles divided into susceptible (S), infected (I), and recovered (R). We use three groups, but the model can account for other categories commonly used in traditional epidemiological models (e.g. exposed or immune). Particles move in a two-dimensional domain $\mathcal{D}$ that represent the environment where the individuals live. In this first example, boundaries are periodic, i.e. particles that exit the domain in one side re-enter it from the opposite side. Random, human motion can be calculated with the Langevin equation (Behera et al. 2020)

$$m\frac{d\mathbf{v}}{dt} = -m\gamma_f \mathbf{v} + F_{REP} + F_{DRIFT} + F_{EXT} + \xi(t), \qquad (1)$$

where, m is the mass of the particle, $\mathbf{v}$ the velocity, and γ_f a friction coefficient. F_{REP} is an interparticle repulsive force that prevents particles from overlapping. F_{DRIFT} keeps particles together when moving in a crowd. F_{EXT} refers to external forces preventing individuals from colliding with obstacles. $\xi(t)$ is a fluctuating force accounting for the stochastic nature of human motion, and it is calculated at each time step by a random number generator with properties

$$\langle \xi(t) \rangle = 0, \ \langle \xi(t)\xi(t+\Delta t) \rangle = \frac{m^2 D\gamma_f}{\Delta t^2}. \qquad (2)$$

The parameter D is a measure of the fluctuation of the trajectory and is estimated for different human activities (e.g., indoors motion, outdoor activities, mass gatherings, etc.) from high-resolution GPS trajectories (Gallotti et al. 2018), or videos recordings (Ali and Shah 2007, Cai et al. 1995). Equation 2 produces a Wiener process, i.e. a random walk where the mean squared displacement (MSD) is proportional to Δt. Lévy processes, where MSD is proportional to Δt^n with $n > 1$, have also been suggested for human mobility (Rhee et al. 2011). For simplicity, we initially consider a Wiener process with $\gamma_f \to \infty$. In this case, eq. 1 reduces to a Brownian walk (Einstein 1905) with $F_{REP} \to 0$, $F_{DRIFT} \to 0$, and $F_{EXT} \to 0$. Each time step, the velocity of every individual is drawn from a normal distribution with mean $\mu = 0$ and variance $\sigma^2 = 2D/\Delta t$, and its position updated accordingly.

Infected particles have a radius of influence r. Every time susceptible individuals move within the radius of influence of an infected one, there is an 'encounter' and the susceptible individual has a certain probability p to become infected (Figure 1).

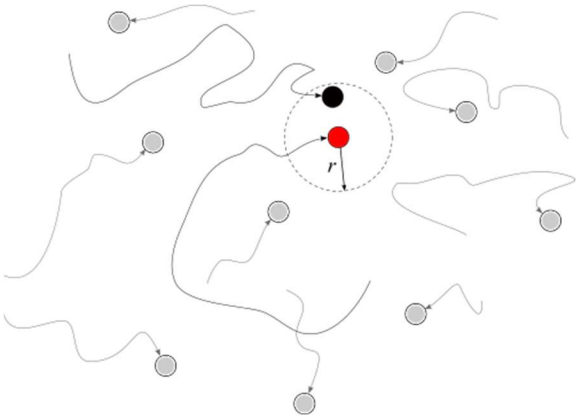

Figure 1. Motion and contagion of individual particles.

This probability is handled in a Monte Carlo fashion: if p is the probability that a contact lasting Δt produces an infection, infection occurs if

$$R_1 < p\Delta t\,, \tag{3}$$

where $R_1 \in [0,1]$ is a random number with uniform distribution. The rate of recovery of infected particles is handled in a similar way. If γ is the recovery rate, an infected individual recovers if

$$R_2 < \frac{\Delta t}{\gamma}, \tag{4}$$

where $R_2 \in [0,1]$ is another random number with uniform distribution. For details on Monte Carlo methods and the theoretical justification of eq. 3 and eq.4, the reader can refer to Rubinstein (1991).

Traditional compartmental models do not account for spatial inhomogeneities: every newly infected individual is automatically 'spread' over the entire domain. The DE model is not 'perfectly mixed' and individuals have positions that change over time. When their mobility is high with respect to the size of the domain, the model replicates traditional SIR models (Figure 2). Mobility is defined by the dimensionless number velocity

$$\mathrm{M} = \langle v \rangle \frac{T}{L}, \tag{5}$$

where $\langle v \rangle$ is the average velocity of the individuals, T a reference time and L a reference length. Here, we use the size of the computational domain (1 km) for L, and one day for T. Thus, M can be thought as the average distance in km travelled by an individual in a day. Both DE simulations in Figure 2 are based on initial conditions N_S = 4069, N_I = 1 and N_R = 0. The time step used in the simulation is Δt = 1 min.

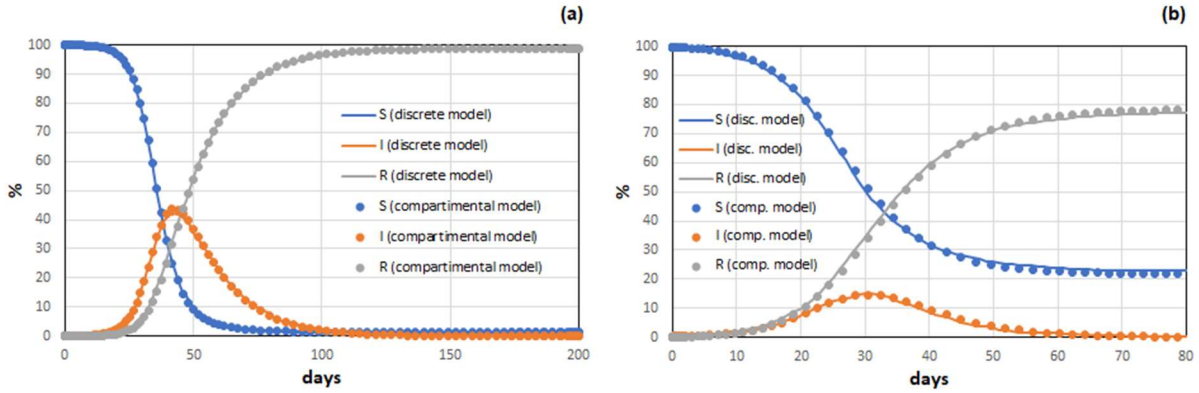

Figure 2. Comparison between the discrete model and the classical SIR model for two different cases: (a) M = 1.3, r = 4 m^{-1}, p = 1/1000 min^{-1}, which corresponds to β = 0.29 day^{-1} in the SIR model (γ = 1/15 day^{-1} for both models); (b) M = 5, r = 1 m^{-1}, p = 1/30 min^{-1}, which corresponds to β = 0.39 day^{-1} in the SIR model (γ = 1/5 day^{-1} for both models)

Figure 2 shows the temporal evolution of a population with high mobility; in this case, the DE model is equivalent to the 'perfectly mixed' SIR model. At low mobilities, individuals move slowly with respect to the size of the computational domain. In this case, the system is far from the perfect mixing assumption of the classical SIR model. The lattice-SIR model (Grassberger, 1983) accounts for this

scenario: individuals do not move and are represented by nodes of a lattice that can infect their immediate neighbours. In DE, low values of M generate patterns typical of the lattice-SIR model (Figure 3). The disease spreads along a front of infection, rather than being evenly distributed (Video 1).

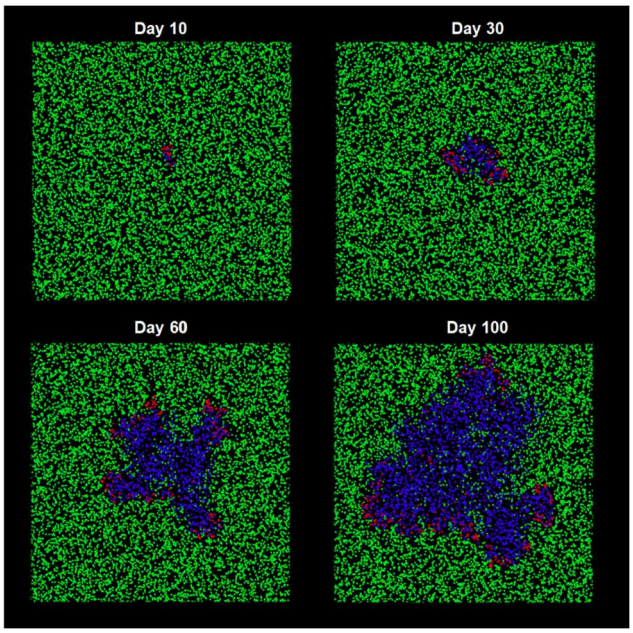

Figure 3. At low mobilities, the discrete model behaves like a lattice-SIR model: M = 0.05, r = 4 m^{-1}, p = 1 min^{-1}, and γ = 1/5 day^{-1}; susceptible individuals are in green, infected individuals are in red, removed individuals are in blue.

Based on the particle mobility, this preliminary DE model replicates both the classic and the lattice-SIR model. We use this feature for modelling policies that limit population's mobility. Parameters like r (contagion distance), p (contagion probability of two individuals within r) and γ (recovery rate) are (at least in theory) intrinsic of the diseases and do not depend on the mobility of the population. Therefore, we consider scenarios where r, p and γ are constant and only M variable.

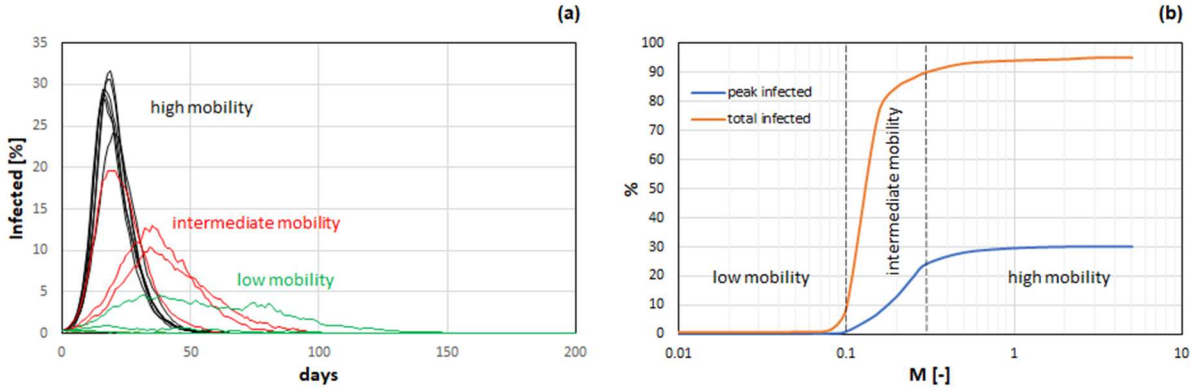

Figure 4. Effect of reducing the mobility of a system with r = 1 m^{-1}, p = 1/30 min^{-1}, and γ = 1/5 day^{-1} on the time series of the infected population (a), and the peak and total number of infected (b). Low, intermediate, and high mobilities regimes correspond to M < 0.1, 0.1 < M < 0.3, and M > 0.3, respectively.

In Figure 4, it is possible to distinguish three different behaviours, or regimes, according to the magnitude of M. If $\mathrm{M} > 0.3$ (i.e. individuals travel an average distance from home higher than 3 km

per day), the system is perfectly mixed: the disease spreads at its full capacity and most of the population gets infected. If $\mathrm{M} < 0.1$ (i.e. individuals travel an average distance from home lower than 1 km per day), the system is segregated: pockets of diseases form, but due to the low mobility, they do not easily spread to neighbour areas. Finally, if $0.1 < \mathrm{M} < 0.3$, an intermediate situation occurs. Figure 4 shows that there is a critical range that dramatically reduces the number of infections. As M goes from 0.3 to 0.1, the total percentage of the infected population decreases from 90% to 10 %.

3. Second model: behavioural inhomogeneities in the population

In the previous model, the mobility reduction affects the whole population in the same way, which is not realistic. A fraction of the population must conserve higher mobility to ensure the functioning of society, and the entire population will not observe the quarantine with the same consistency. Standard epidemic models assume that all individuals behave in the same way, but DE models do not have this limitation. This second DE model divides the population into two groups: those who observe the lockdown and have low mobility, and those who do not observe the lockdown and maintain higher mobility. We assume that the population with high mobility has $\mathrm{M}_{\mathrm{high}} = 0.3$ and the population with low mobility $\mathrm{M}_{\mathrm{low}} = 0.1$. In the simulations, we vary f, the fraction of individuals with high mobility over the total population and calculate the effect of f on the number of infected. The parameters that characterize the diseases are the same as the previous section (r = 1 m^{-1}, p = 1/30 min^{-1}, and γ = 1/5 day^{-1}) with 20 initial infected individuals randomly distributed between the two populations.

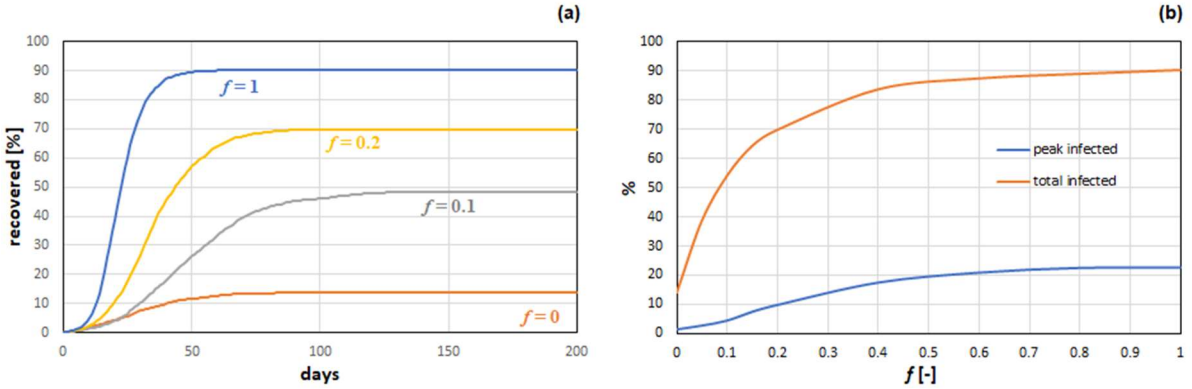

Figure 5. Effect of the fraction f of high mobility individuals on a system with r = 1 m^{-1}, p = 1/30 min^{-1}, $\mathrm{M}_{\mathrm{low}}$ = 0.1, $\mathrm{M}_{\mathrm{high}}$ = 0.3, and γ = 1/5 day^{-1} on the time series of the recovered population (a), and the peak and total number of infected (b).

Figure 5 shows that the total number of infections strongly depends on f. It is enough that 10% of the population does not reduce its mobility to increase the number of total infected from 15% to 50%.

4. Third model: masks and social distancing

According to the literature, the efficiency of masks in reducing spreading is between 58% and 85% (Brienen et al. 2010). In the model, this is accounted for by a fraction of the populations with high mobility wearing the mask. We start from the example of Section 3 with $f = 0.2$ and consider that a fraction s of the $\mathrm{M}_{\mathrm{high}} = 0.3$ population wears a mask. Wearing a mask changes p. While in the previous example all individuals have the same p, in this case, p is smaller for individuals wearing the mask. Assuming 70% mask efficiency: if p is the probability of infection without mask, $0.3p$ is the probability of infection wearing the mask.

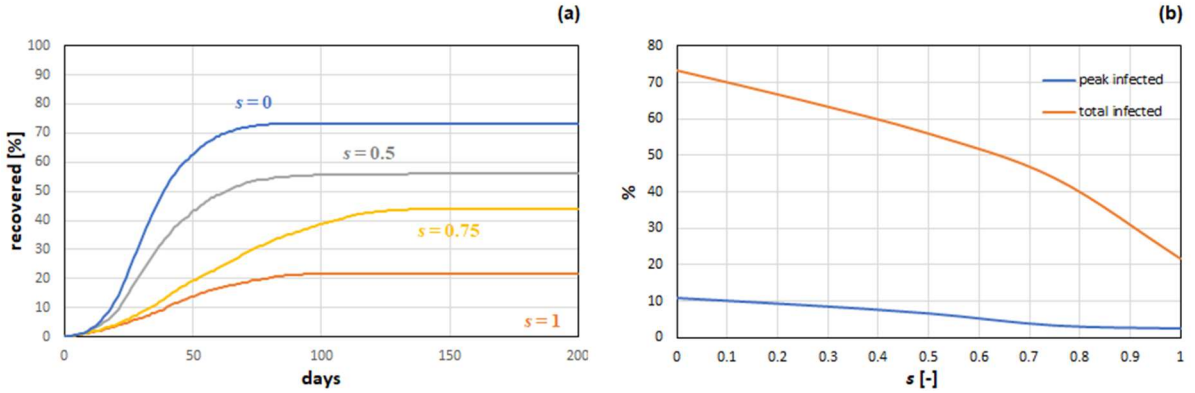

Figure 6. Effect of the fraction *s* of people with high mobility wearing mask on a system with r = 1 m^{-1}, p = 1/30 min^{-1}, M_{low} = 0.1, M_{high} = 0.3, f=0.2, and γ = 1/5 day^{-1} on the time series of the recovered population (a), and the peak and total number of infected (b).

Figure 6 shows that mask can be effective, but the fraction of people with high mobility (i.e. interacting with other individuals on a regular basis) wearing them should be >50%. This is another 'toy model', but, despite its simplicity, it highlights some advantages of DE. The mask efficiency is retrieved from the literature and added to the model by 'first principles'. We do not need to recalculate or reassess any parameter from new data as in traditional epidemiological models.

In the previous models, there is no limit on how close particles can approach each other. We can model social distancing with a repulsive force $F_{REP} > 0$ in eq. 1. To achieve this goal, we introduce a potential known in MD as 'soft repulsive potential'

$$U = \begin{cases} A\left[1+\cos\left(\frac{\pi r_p}{r_c}\right)\right] & r_p < r_c \\ 0 & r_p \geq r_c \end{cases}, \qquad (6)$$

where r_p is the distance between two particles, r_c a cut-off distance, and A the rigidity of the potential. This potential produces a repulsive force

$$F_{REP} = -\nabla U, \qquad (7)$$

which tends to keep particles at a distance $r_p > r_c$. We use $r_c = r$, which means that individuals try to keep a distance that is larger than the infection radius r. However, because the potential is soft, there are times when this does not occur. The lower the value of A, the softer the potential, and the less likely is for two particles to maintain the prescribed distance. In MD, atomic distances are shown with the radial distribution $g(r_p)$, i.e. the probability to find a particle at a distance r_p from a given reference particle. Figure 7a show $g(r_p)$ for different values of A. If $A = 0$, there is no repulsion, $F_{REP} = 0$ and $g(r_p)$ is flat, which means that all distances between individuals are equally probable. As A increases, it becomes less likely to find two individuals at a distance lower than r, which decreases the probability of contagion (Figure 7b).

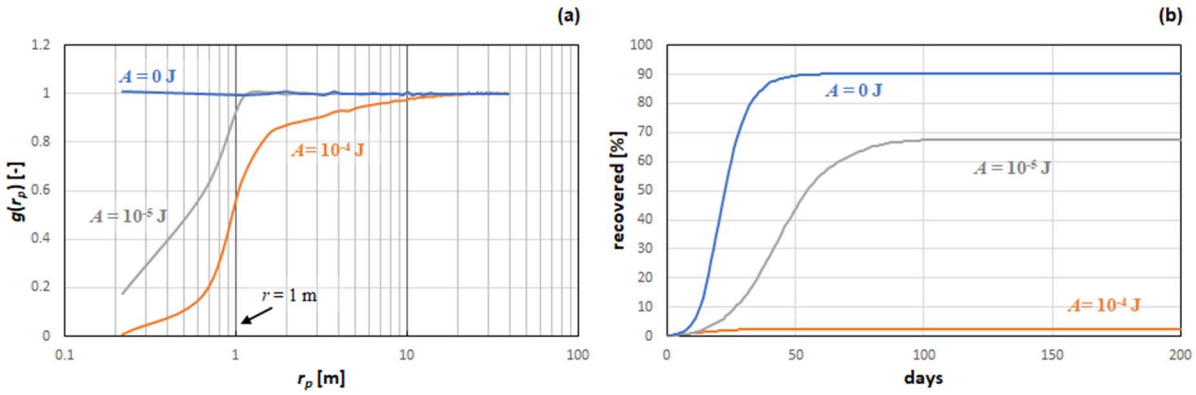

Figure 7. Effect of social distancing on a system with r = 1 m^{-1}, p = 1/30 min^{-1}, M = 0.3, and γ = 1/5 day^{-1}: radial distribution function (a) and recovered population (b).

5. Fourth model: gathering spots (workplaces, schools etc.)

In this section, we consider the presence of a gathering spot such as a workplace or a school in the domain.

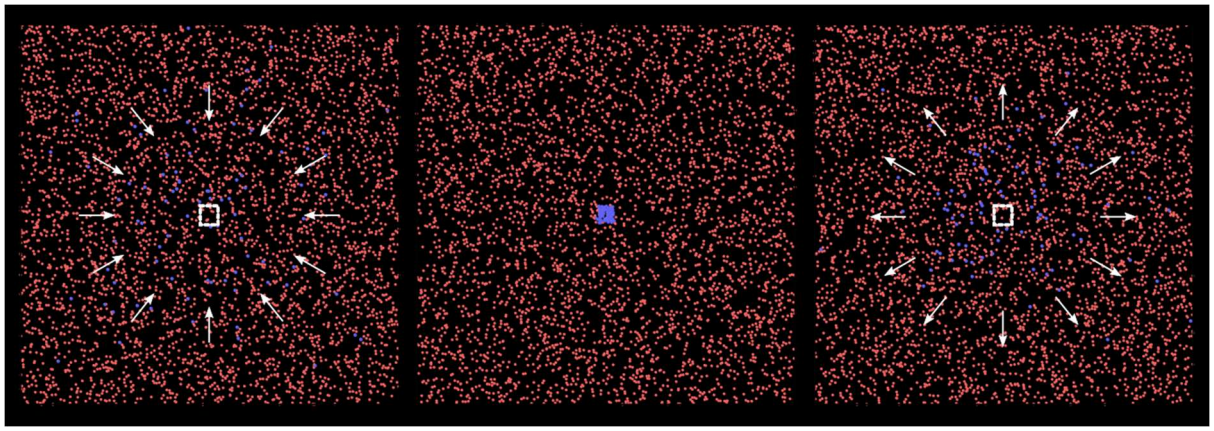

Figure 8: A fraction of particles is pushed towards a gathering spot in the centre of the domain for eight hours a day to model the presence of a school or a workplace.

A periodic force F_{EXT} in eq. (1) is used to push the particles inside a region in the centre of the domain (Figure 8) and keep them there for eight hours every day. After this time, their normal mobility ($\mathrm{M} = 0.1$) is reintroduced. In this toy model, we have a single gathering spot, which is visited by 2% of the particles (blue particles in Figure 8) randomly selected at the beginning of the simulation. The rest of the population has low mobility ($\mathrm{M} = 0.1$) and does not visit the gathering spot unless they randomly move to the central area of the domain. All other simulation parameters are the same as Figure 4.

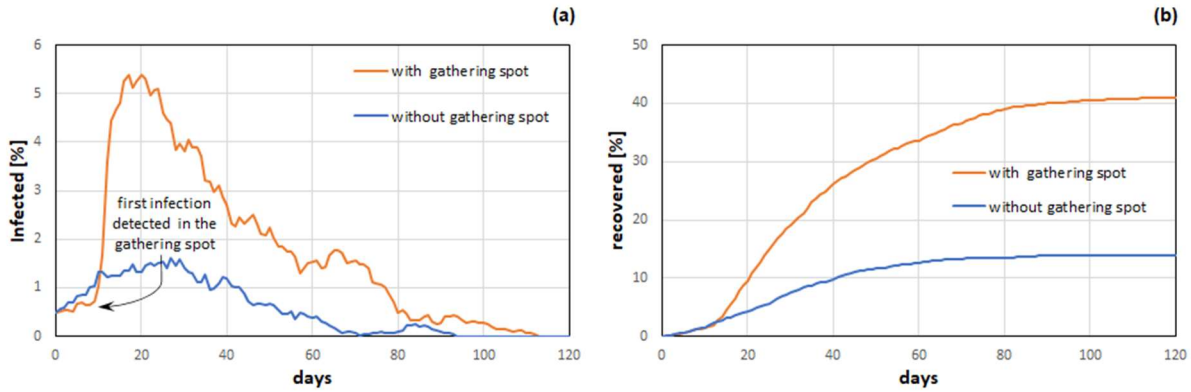

Figure 9. Effect of a gathering spot on a system with r = 1 m^{-1}, p = 1/30 min^{-1}, M = 0.1, and γ = 1/5 day^{-1} on the infected (a) and recovered population (b).

Figure 9 shows the effect of the gathering spot on the infected population. During the first week, the effect looks beneficial. Part of the population gathers for eighth hours a day in the same spot. As long as no infection occurs here, the probability of contagion from outside is lower. However, after the first individual is infected, the rest of the population visiting the communal area follows suit. This produces a peak of infections that spreads to the entire population.

6. Fifth model: spatial inhomogeneities (city and countryside)

All models considered so far assume that the population density is the same in the whole domain. This is hardly the case as, for instance, cities have a higher population density than their countryside. The next toy model assumes that the population density in one region of the domain is higher than the rest.

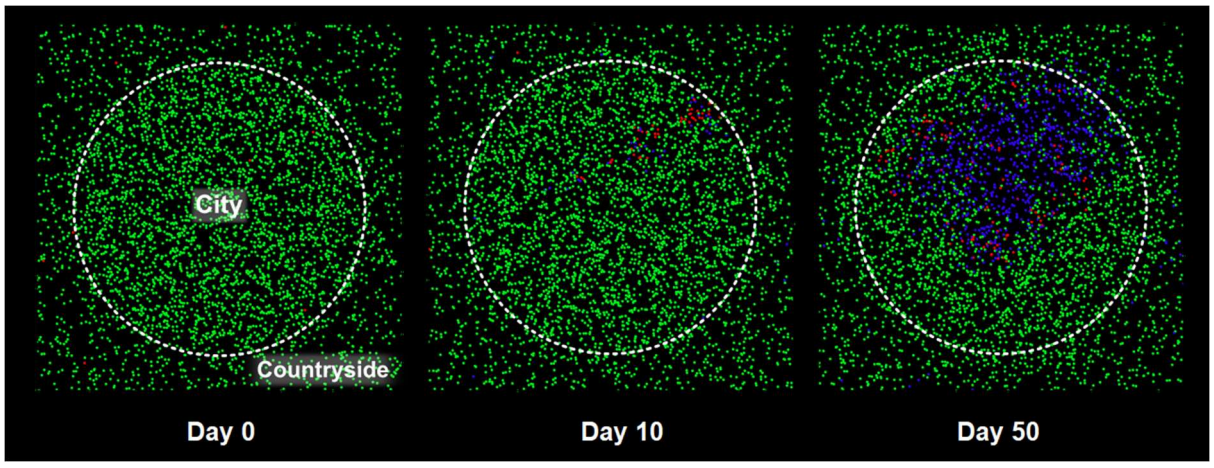

Figure 10. Evolution of a system with city/countryside density difference: r = 1 m^{-1}, p = 1/30 min^{-1}, $\mathrm{M} = 0.1$ and γ = 1/5 day^{-1}; susceptible individuals are in green, infected individuals are in red, removed individuals are in blue.

In Figure 10, the circle in the centre of the domain is the city, the rest the countryside. The total number of particles in the domain is the same as the previous examples, but they are distributed differently with the city having a population density double than the countryside. Particles can cross the city boundaries, but an 'invisible wall' reflects some of them to maintain the population densities in the two regions at the prescribed values.

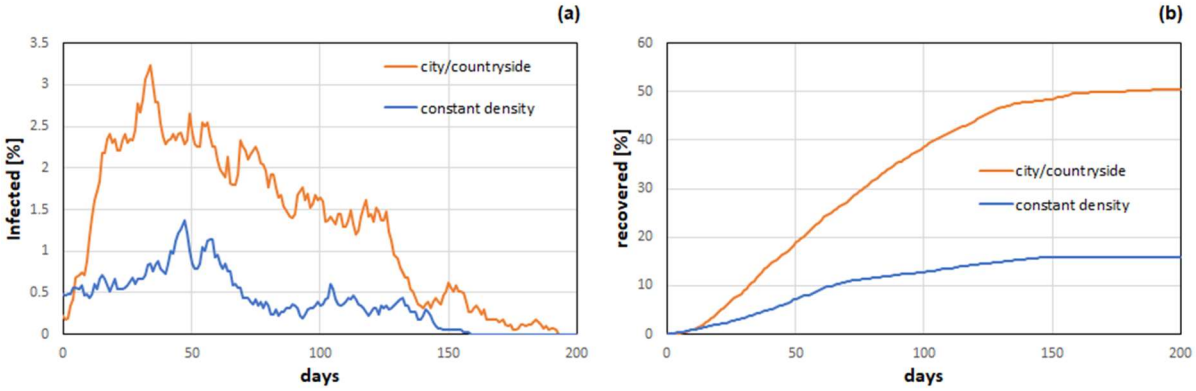

Figure 11. Effect of a population density difference between city and countryside on a system with r = 1 m^{-1}, p = 1/30 min^{-1}, $\mathrm{M} = 0.1$ and γ = 1/5 day^{-1} on the infected (a) and recovered population (b).

Figure 11 compares the result of this model with that of uniform density (the same as Figure 4). The presence of a region at higher density increases the total infections from 15% to 50%.

7. Sixth model: temporal inhomogeneities (day and night)

This model considers that individual mobility is lower at night. This is achieved by changing the mobility of the particles during the 24 hours. The velocity of the particles is always drawn from a Gaussian distribution with mean $\mu = 0$ and standard deviation $\sigma = v$. However, while in all previous models v is constant, it now varies during the 24 hours according to

$$v(t) = \frac{\pi}{2}\langle v\rangle \left|\sin\left(\frac{\pi t}{T}\right)\right|, \qquad (8)$$

where $\langle v\rangle$ is the constant standard deviation used in all previous examples, and the period T is equal to one day. Equation (8) guarantees that the average mobility during the 24 hours is the same as before. However, instead of being constant the whole time, it is maximal in the middle of the day and drops at night. Figure 12 compares time-dependent mobility (average $\langle \mathrm{M}\rangle = 0.1$) with the constant mobility (always $\mathrm{M} = 0.1$).

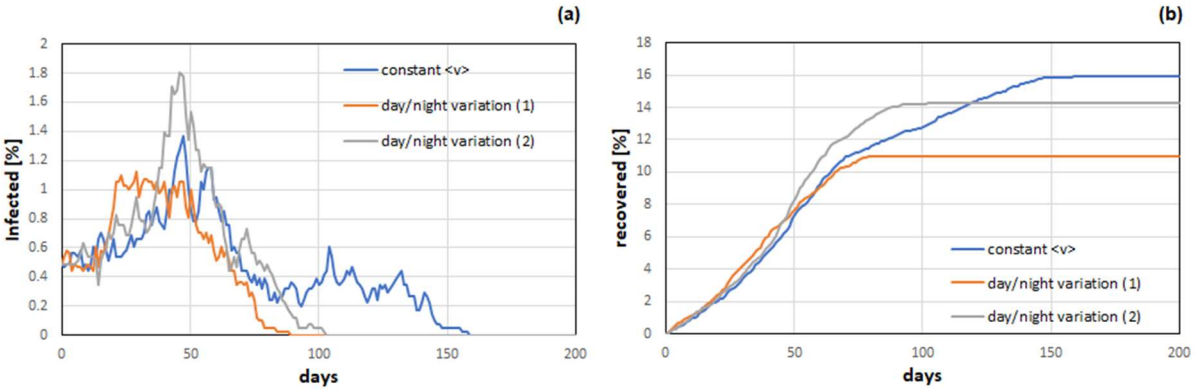

Figure 12. Effect of day-night mobility variations on a system with r = 1 m^{-1}, p = 1/30 min^{-1}, $\langle \mathrm{M}\rangle = 0.1$, and γ = 1/5 day^{-1} on the infected (a) and recovered population (b).

Perhaps surprisingly, the simulation with day/night variation shows a lower infection. However, the stochastic nature of the model plays a role here. If the simulation is repeated with a different initial random distribution of infected particles, the results are somewhat different (grey line in Figure 12).

Technically speaking, all results (especially those at low mobilities) should be repeated several times with different random numbers to assess the probability of each outcome. Since the toy models are only meant to introduce the main features of DE, this is not carried out.

8. Seventh model: homes and families

So far, we did not consider people returning home at night. To account for this, we use an additional F_{EXT} in eq. 1 that, between 8:00 pm and 4:00 am, keeps each particle at 'home' (the initial particle position). Conceptually, the approach is similar to Section 5, but now F_{EXT} moves particles back to their individual home rather than towards a gathering point. Ambiguities on the direction of 'home' may arise with periodic boundary conditions. Therefore, the box boundaries are switched to 'reflective'. Particles moving outside the box by a certain distance are put back inside by the same distance with the sign of the corresponding velocity component flipped. Figure 13 shows that 'homes' with single occupants tend to suppress the infection. By returning to their initial position every night, particles visit a smaller portion of the domain. The model is extended to consider 'families', i.e. multiple occupants sharing the same home. Several particles share the same initial position (just shifted a few meters to avoid overlapping) to reproduce a target average household size. Here, we assume a household size of 2.56 (Birmingham's value). Families produce a different effect according to the mobility of the particles (Figure 13). Low mobilities ($\langle M \rangle = 0.1$) result in an initial spike of contagions because people sharing the same house can easily infect each other. However, after that, the infection rate decreases sharply. In fact, by lumping particles together, the average distance between individuals belonging to different households increases, decreasing the probability of contact. However, high mobilities ($\langle M \rangle = 0.3$) compensate for the higher distance. In this case, the spike is not followed by a reduction of infections as for low mobilities.

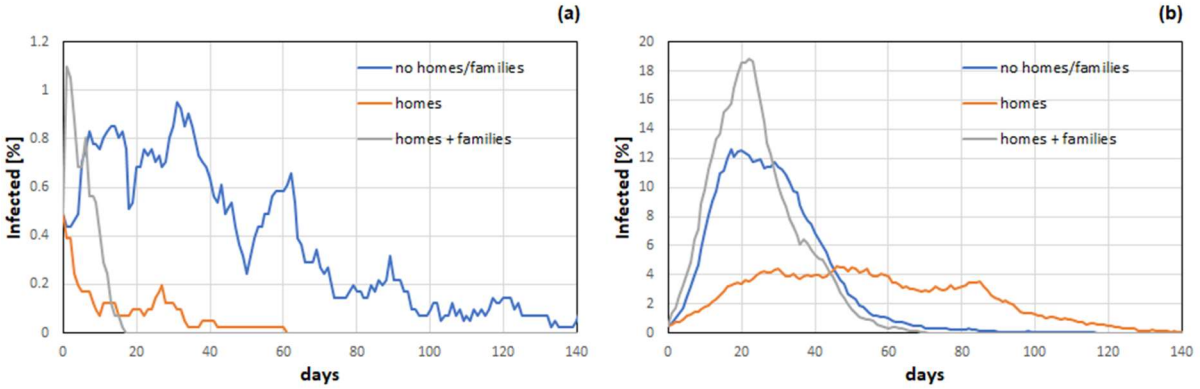

Figure 13. Effect on the infected population of the addition of homes and families in the model for a system with r = 1 m^{-1}, p = 1/30 min^{-1}, and γ = 1/5 day^{-1} in the case of (a) $\langle M \rangle = 0.1$ and (b) $\langle M \rangle = 0.3$.

9. Eighth model: public transport, and streets

In this model, we consider two separate regions of 2,000 particles separated by an empty zone. For reference, we call the upper region the 'northern village', and the lower region the 'southern village'. Particles have variable day/night mobility as in Section 7 and return home at the end of the day as in Section 8. All particles infected at $t = 0$ are in the southern village (Figure 14). If there is no connection between the two regions, and since particles have low mobility ($\langle M \rangle = 0.1$), the epidemic lasts 20 days and only a small fraction of the population of the southern village is affected. Since the two villages are separated, the infection has no mean of spreading to the northern village.

The previous scenario is modified by assuming that the two villages are connected by rail. 'Home' and 'working-place' positions of each particle are selected randomly at the beginning of the simulation. Two hundred particles from the southern village are allocated to the group 'commuters'. Their home is in the southern village and their working-place in the northern village. Every morning, commuters move to the northern village and go back home during the evening by train. Mathematically, the collective movement of individuals using the train is modelled as a force field (a space dependant F_{EXT} in eq. 1) that directs a fraction of the southern population to the north in the morning and then back to the south in the evening. In the case under investigation, this force field is expressed as

$$F_{EXT}(x,y) = \left(-xf_x, f_y\right), \qquad (9)$$

where f_x and f_y are determined to set the travelling time to the wanted value (1 hour in this example). Equation 9 constrain particles to follow a given path (the train line) and it is only applied for the duration of the outward journey. After the particles arrive in the northern village, the force field is substituted by a F_{EXT} that moves the particles to their working places, as in Section 5. Once particles reach their working place, for the next eight hours, no additional force is applied, and they move based on their background mobility ($<M> = 0.1$). At the end of the working day, eq. 9 is applied in the opposite direction to simulate the return journey. Finally, an additional force drives the particles home for the night, as in Section 5. Video 2 shows the evolution of the infection in detail.

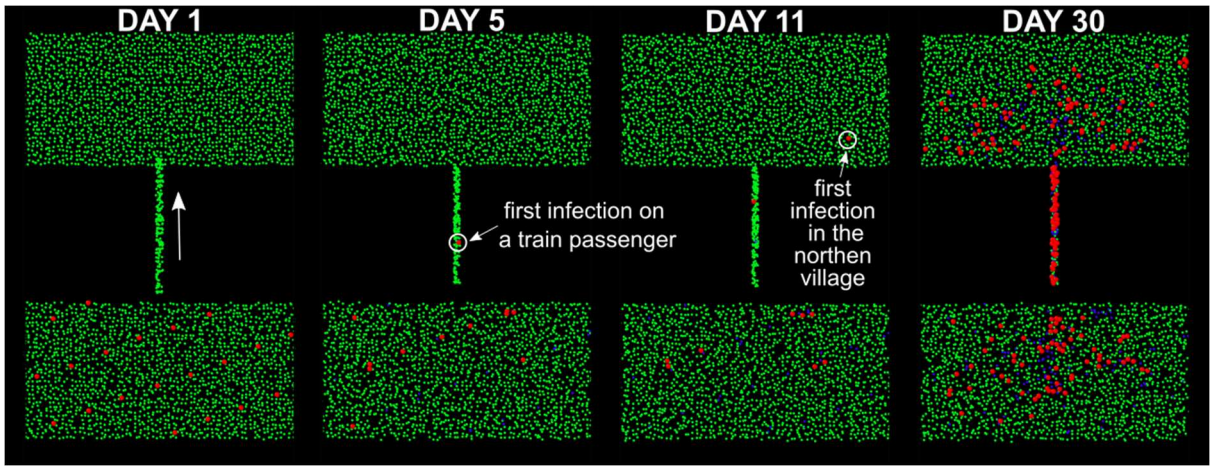

Figure 14. Evolution of two separated systems with 200 commuters moving between the two regions: r = 1 m^{-1}, p = 1/30 min^{-1}, $<M> = 0.1$ and γ = 1/5 day^{-1}; susceptible individuals are in green, infected individuals are in red, removed individuals are in blue. For graphical reasons, the size of the dots representing infected individual is eight times larger than that of susceptible and recovered individuals.

The presence of the train increases dramatically the spread of the disease for two reasons. Firstly, passengers in the train are at close contact increasing the chances of infection. Secondly, they bring the infection to the other village. Figure 15 compares the scenarios with and without train passengers.

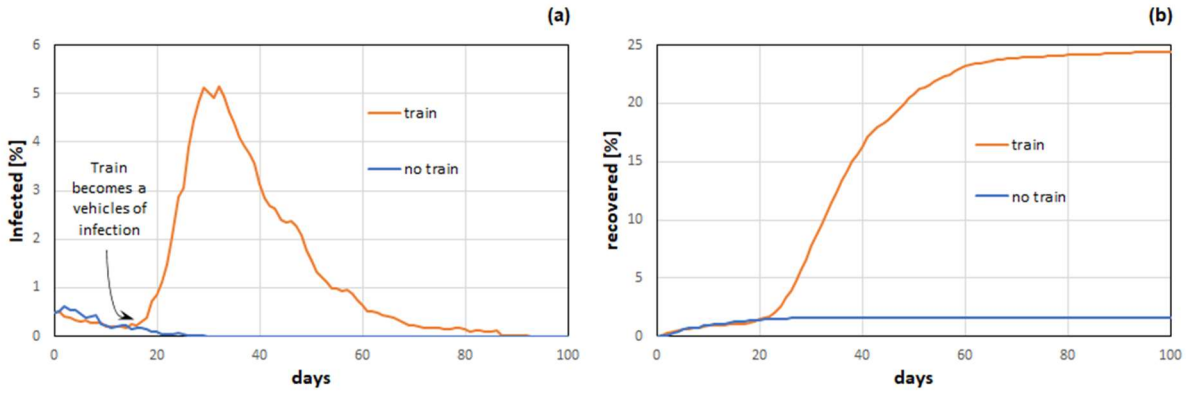

Figure 15. Effect of 200 commuters moving between two regions on a system with r = 1 m^{-1}, p = 1/30 min^{-1}, $\langle M \rangle = 0.1$, and γ = 1/5 day^{-1} on the infected (a) and recovered population (b).

A similar idea can be used to model the presence of buses in the city. Commuters that use a specific bus line are subjected to time-dependent force fields (e.g. Figure 16) that constrains them to follow a given path. The force field is only used for commuters that use public transportation and find themselves at close contact with other passengers. Buses are discussed in detail when modelling Bogotá.

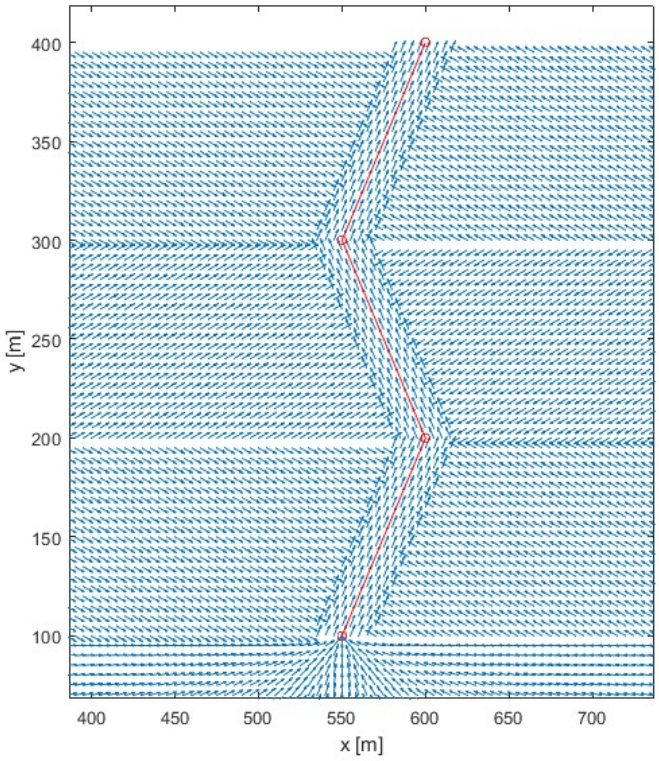

Figure 16. Example of 'force field' used to constrain particles within a given path or street (red line)

10. Putting all together 1: simulating the city of Birmingham, UK

This section puts together all ideas developed so far to simulate Birmingham in the UK (~1 million inhabitants). The first step is to digitally recreate the area of the city and its boundaries framed in a computational box of side 30 km. The area between the city and the box is the countryside. Boundary

conditions at the box are 'reflective' as discussed in Section 8. Particles are free to move from the city to the countryside and vice-versa.

After the geometry is set, the next step is to generate its virtual population. The population density of the city is 3,649 inhabitant km^{-2}, while the surrounding countryside has 456 inhabitants km^{-2}. For simplicity, density differences within the city are ignored. This generates 1,072,924 particles each representing a digital inhabitant: 960,483 inside the city and 112,441 in the countryside. Particles are arranged on a randomly perturbed lattice. The initial location of each particle is labelled as 'home' and the average household size 2.56 (Birmingham City Council, 2011) as discussed in Section 8. In theory, we could use the exact locations of all households in Birmingham, but this is left for future versions of the model.

The third step consists in generating the individual properties of each particle affecting either its mobility or susceptibility to the disease. An age is randomly attributed to every individual according to the statistical age distribution in the UK (Park, 2020). In average, an individual in the UK walks around 1 km per day (Department of Transport, 2019). This mobility is accounted for as random walk as in Section 2. The population is further divided into employed, pupils and unemployed. Individuals are randomly allocated to these groups according to employment statistics based on age groups (Watson 2019) shown in Table 1.

Table 1: Percentage of the employed population in the UK within age groups

Age group	% of employed
16 to 24	74.5
25 to 34	84.3
35 to 49	85.4
50 to 64	72.7
16 to 64	76.1

For each member of the employed and pupil group, a location on the map is assigned as, respectively, working place or school. At this stage, these locations are random: the painstaking task of specifying the exact locations of all working places and schools in Birmingham is left for future versions of the model. During the day, the particle goes to this location (as discussed in Section 5) and returns home in the evening (as discussed in Section 8). This additional mobility is applied only for the time required to reach its destination and is added on top of the 1 km day^{-1} mentioned before. Since 10% of the working population works from home (Bela and Wilkinson, 2020), this mobility bonus is not given to 10% of the employed group selected randomly. According to statistics, the average distance of an individual from work is 10 km (UK Data Service, 2011) and of a pupil from school is 3 km (Department of Transport, 2014). Distances between home and work and home and workplace are randomly assigned to each individual according to these statistics. The time of the day when commute from and to work occurs is different for each individual and allocated randomly based on the distributions shown in Figure 17c and 17d. We could not find precise statistics for these times, which, therefore, are based on common sense.

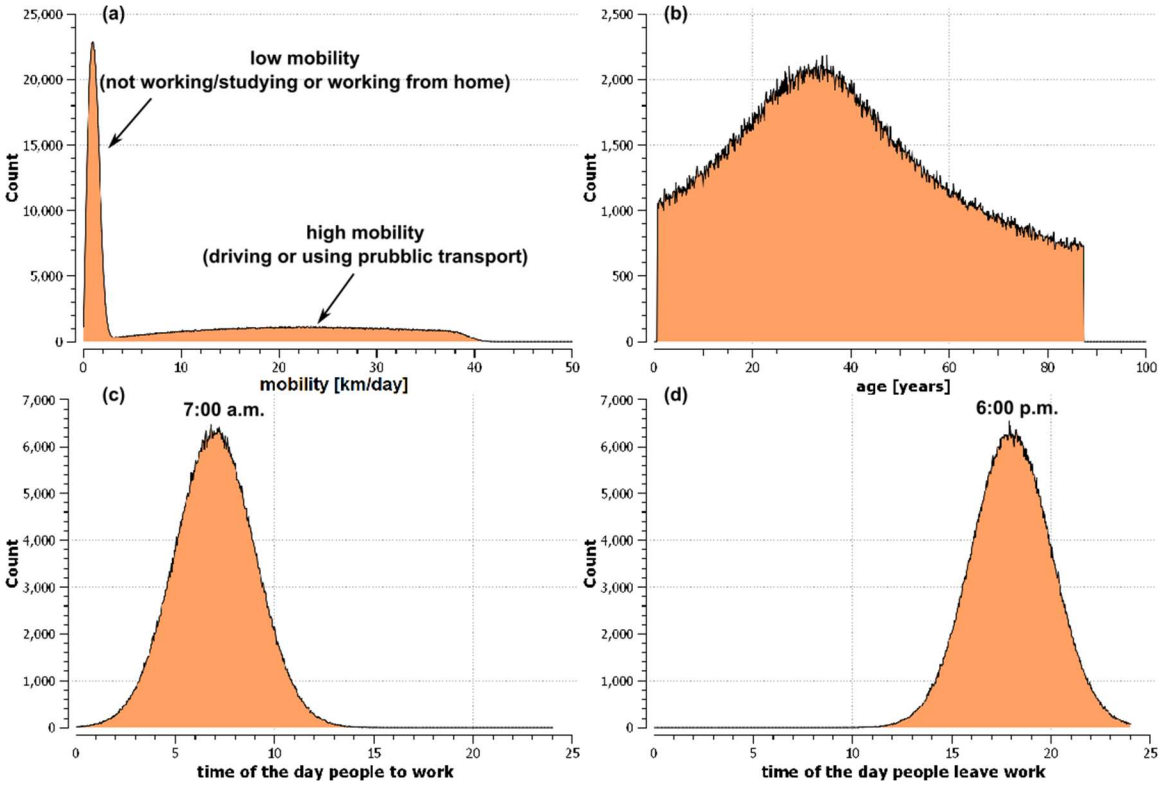

Figure 17. Some of the statistics of the virtual population used in the simulations: (a) mobility, (b) age, (c) time of the day when people go to work, (d) time of the day when people leave work

The probability of interacting with other individual is higher if commute occurs by means of public transportation. Several 'nodes' (e.g. bus, train stations) where commuters congregate are created on the map. Two-thirds of the working population use these nodes (West Midlands Combined Authority, 2017); the remaining third drives to work and, therefore, do not transit through these nodes. Future versions of the model could account for the exact place all nodes (e.g. bus, train stations); in this study, for simplicity, 300 nodes are created at random locations.

Based on the description above, at any given time, an individual can have either low mobility, which represents an individual staying at home or walking near home (average distance 1 km day^{-1}), or high mobility, which represents a particle commuting to work (average distance 10 km day^{-1}) or school (average distance 3 km day^{-1}). However, according to the statistics (Department of Transport, 2018), during the day, there are 400,000 vehicles on Birmingham's streets. While employed individuals are at work and pupils at school, the mobility of a fraction (chosen randomly) of the remaining population is increased to 10 km day^{-1} to simulate people driving for reasons other than commute (e.g. shopping, leisure etc.). This additional mobility is added as a random walk (Section 2) and considering day/night differences (Section 7).

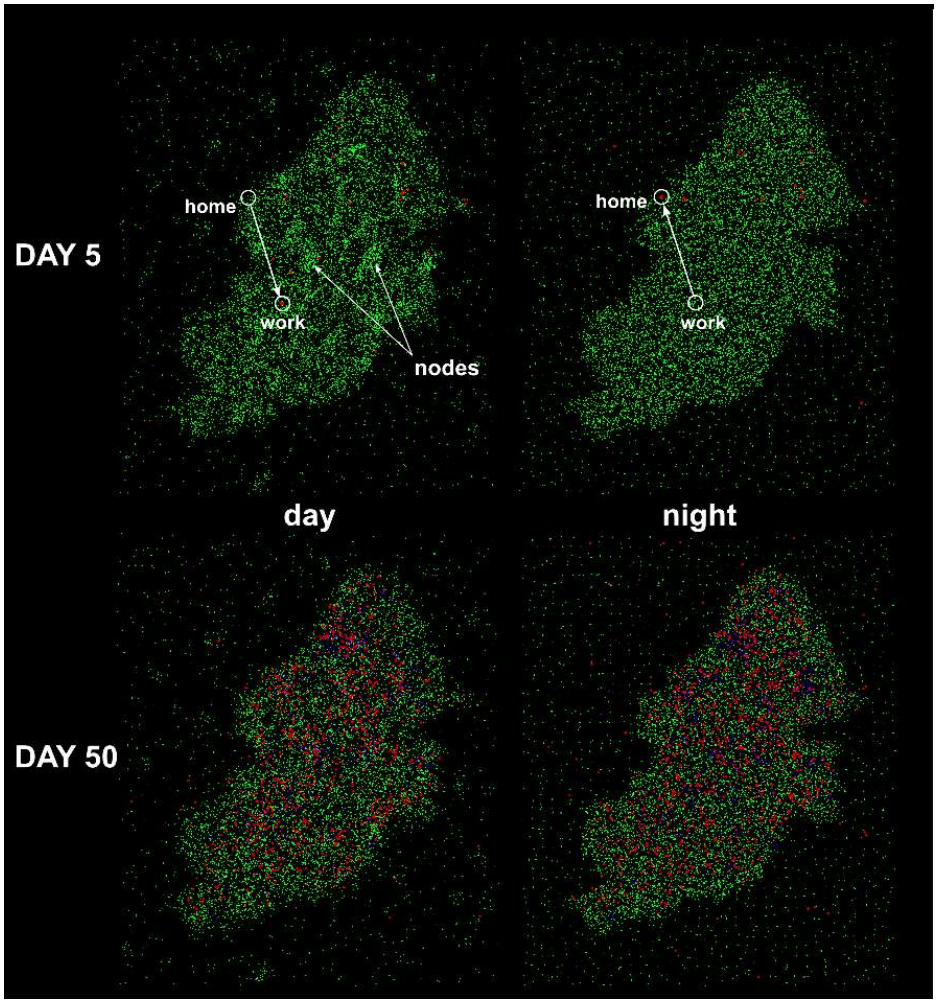

Figure 18. Infection dynamics in the virtual Birmingham and its surroundings. For graphical reasons, only 1% of the population is represented and the size of the dots representing infected individual is ten time larger than that of susceptible and recovered individuals. An example of home-work commuting and a few 'nodes' are highlighted.

Besides the city and its population, we need to model the disease. Here, we use $r = 2$ m and $\gamma = 1/7$ day^{-1}, which have been suggested for covid-19 (Pamieri et al., 2020; CDC, 2020). The parameter p is used to adjust the model's response when no policy against the epidemics is implemented. It accounts for features that are not directly considered in the model and must be 'captured' from real data. This includes the probability that infected individuals are identified and, therefore, it also depends on the quantity and quality of testing carried out in the city. The value $p = 5{\cdot}10^{-3}$ min^{-1} brings a basic reproduction number $R_0 = 2.4$ that is consistent with Birmingham's data during the initial phase of the infection (Government Digital Service, 2020).

The final step consists in running the simulations that cover 200 days with a time resolution of 1 min. They are carried out with the software LAMMPS (Large-scale Atomic/Molecular Massively Parallel Simulator) (Plimpton 1995), a MD program that can be repurposed for generic particle-based simulations. In terms of hardware, we use BlueBEAR, University of Birmingham's supercomputer for high-performance computing (HPC) and high-throughput computing (HTC). Each simulation uses 120 Dual IBM POWER9 CPUs. For one million particles, the duration of each simulation is between one and two hours.

Figures 18 and 19 show the spatial and temporal evolution of the diseases in the virtual Birmingham for the 'business as usual scenario'. Video 3 shows the particles' mobility for 24 hours: every second of video represents 40 real minutes; particles with high mobility have a lighter colour. The video also shows the trip from home to work of a single particle in yellow. Video 4 shows the evolution of the infection: every second of video represents 2 days. In both videos, for graphical reasons, only 1% of the particles is shown. Figures 19a and 19b show the overall evolution of the infected and recovered population. Figure 19c shows that at the end of the epidemics, the city is hit harder than the countryside.

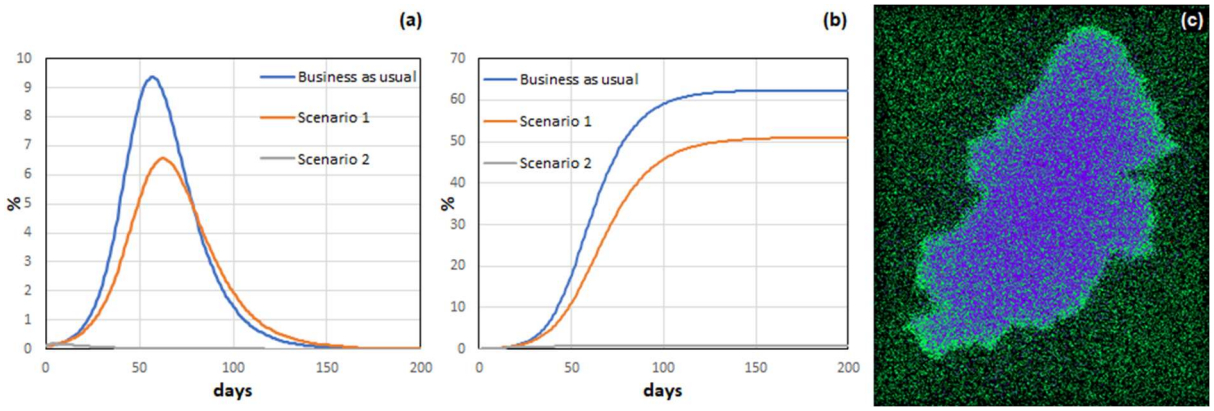

Figure 19. Time evolution of (a) infected and (b) recovered populations for three Birmingham scenarios; (c) spatial distribution of susceptible and recovered population for the 'business as usual scenario' after 200 days (only 1% of the particles is shown).

We can distinguish two factors that determine how the infection spreads within the city. The first is the 'targeted mobility' that accounts for time-recurring trips to specific locations (e.g. school, work, train stations etc.), which, mathematically, is simulated with directional forces (Section 5) or force fields (Section 9). The second is the 'background mobility' that accounts for trips that do not occur every day and are not predictable a priori (e.g. shopping, leisure, etc.), which are simulated by random walks (Section 2). In the 'business as usual' scenario, individuals can be roughly divided into four groups according to the level of their background and targeted mobilities (Figure 20). The model can be used to evaluate the relative importance of the two mobilities on the spreading of the infection. This can be achieved by comparing the 'business as usual' scenario with two other 'extreme' scenarios (Figure 20). In Scenario 1, the individuals conserve their background mobility from the 'business as usual' scenario, but the targeted mobility is completely removed. In this scenario, there are no restrictions to the population movements, but all workplaces, schools and public places are closed. Scenario 2 is the opposite: the background mobility is reduced to a minimum (0.1 km day^{-1}), but the targeted mobility is the same as the 'business as usual' scenario. In this case, workplaces and public places are regularly open, but except for travelling to these places, population' mobility is severely restricted. These are extreme and somehow unrealistic scenarios but are useful for weighing the respective role of the background and targeted mobilities. Figure 19 compares the infected and recovered populations of Scenario 1 and 2 with the 'business as usual' scenario. Both scenarios decrease the total number of infections but reducing the background mobility is more effective. This can be explained by the conceptual difference between targeted and background mobility. Targeted mobility is predictable: it accounts for individuals going always to the same places (e.g. home and workplace) and meeting always with the same people (e.g. family members and

colleagues). Therefore, the pool of potential interactions is limited. In contrast, background mobility has a potentially unbounded stochastic component. In theory, a particle moving only with background motion can approach and infect any other particle in the computational domain and, therefore, its spreading potential is higher.

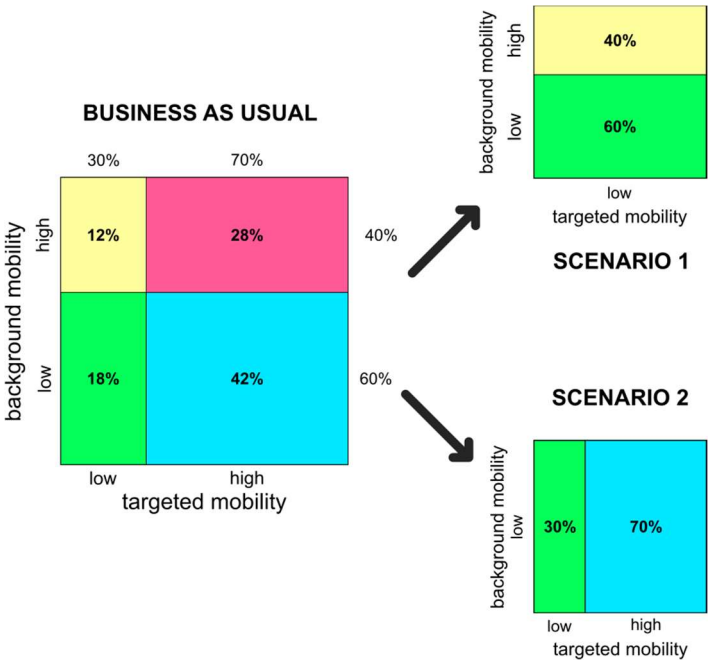

Figure 20. Three scenarios for the city of Birmingham.

The final part of this section shows how the model performs against real data of the covid-19 infection in Birmingham. Figure 21 compares the real data with the 'business as usual' scenario initialized with 5 initial infected individuals randomly distributed in the population. Real data are shown as a 7-days moving average.

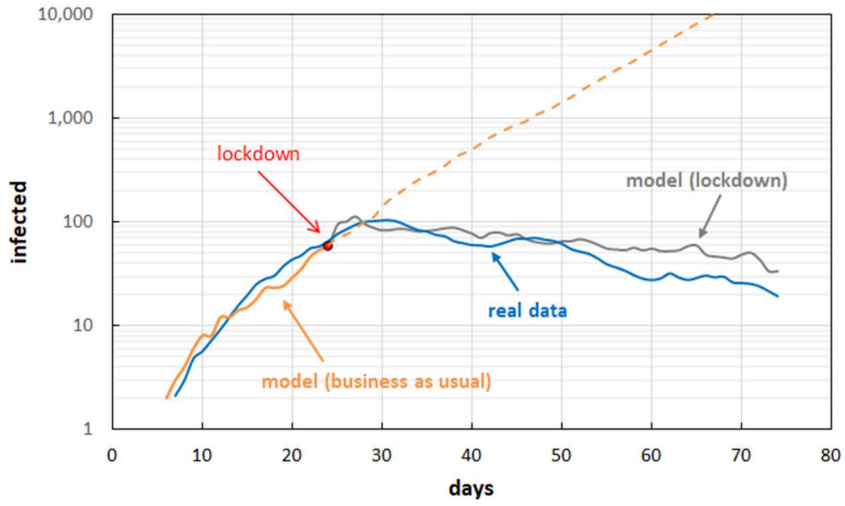

Figure 21. Comparison between real data (7 days moving average) and model output

The 'business as usual' model correctly simulates the data until the day of the lockdown. This is not surprising because the parameter p was chosen to fit the real data. What makes the DE model superior to traditional epidemiological models is the handling of the lockdown. During the lockdown,

both the targeted and the background mobility of the population are reduced. Google made available 'Mobility Reports' that show movement trends (based on requests for directions in Google Maps) over time by geography, across different categories of places such as retail and recreation, groceries and pharmacies, parks, transit stations, workplaces, and residential (Google 2000). We can use these data as an estimate of the reduction of mobility during the lock-down. The Mobility Report for the West Midlands (Birmingham's metropolitan county) indicates that the drop in mobility during the lockdown for 'retail and recreation', and for 'workplaces' was, respectively, 79% and 58%. We feed these data into the model by reducing the background mobility and the targeted mobility by the same amount. This is achieved by reducing by 79% the number of individuals with high background mobility (10 km day^{-1}) and by 58% the numbers of individuals going to work every day; additionally, schools are closed and all trips to and from schools are cancelled. These modifications are applied after day 23; so that the simulation follows the 'business as usual' model until the day of the lockdown and the 'lockdown model' after its implementation. Figure 21 shows that the simulation compares well with the real data. This agreement is achieved with only one adjustable parameter p, which can be considered as a property of the city and estimated at the beginning of the infection. Since p is decoupled from the mobility, it does not change when the lockdown is implemented. Therefore, the model can predict the effect of the lockdown only based on 'first-principles'. That is features that are measurable (e.g. with the Mobility Reports) and have a direct connection with the intended target of the lockdown policy (e.g. the population drop in mobility).

11. Putting all together 2: simulating the city of Bogotá, Colombia

Bogotá has 8.3 million inhabitants. The population is distributed very unevenly (Figure 22a). In the models, we divide the city in three zones (Figure 22b): zone 1 with density 20,000 inhabitants km^{-2}, zone 2 with density 5,000 inhabitants km^{-2}, and zone 3 with density 20,000 inhabitants km^{-2}. This results in a virtual population of 8,292,632: 1,480,928 in zone 1; 1,115,416 in zone 2; and 5,710,748 in zone 3. The average household size is 3.9, which is handled as in Section 8. The background mobility (0.7 km day^{-1}) is estimated from Althoff et al. (2017). Data on age distribution and percentage of the employed population within age groups are taken from (Departamento Administrativo Nacional de Estadistica, 2017) and (OECD iLibrary, 2018) and managed as in Section 10. Modelling transmissible diseases in Bogota also requires considering the socioeconomic structure of the city. As Figure 22c shows, the work-related activities in Bogotá are concentrated in zone 2 (Guzman et. al. 2017), where there are more than 785.000 enterprises registered. The majority, 96.9%, are micro-enterprises (10 employees or less), 2.3% are small enterprises (11-50 employees), 0.53% are medium-sized enterprises (51-200 employees), and 0.24% are big enterprises (more than 200 employees). As a first approximation, we consider all employers concentrated in zone 2, while zone 1 and 3 are modelled as residential districts. The occupation rate also differs in the three zones (Figure 22d); we assume 55% occupation rate in zone 1, 60% in zone 2 and 40% in zone 3.

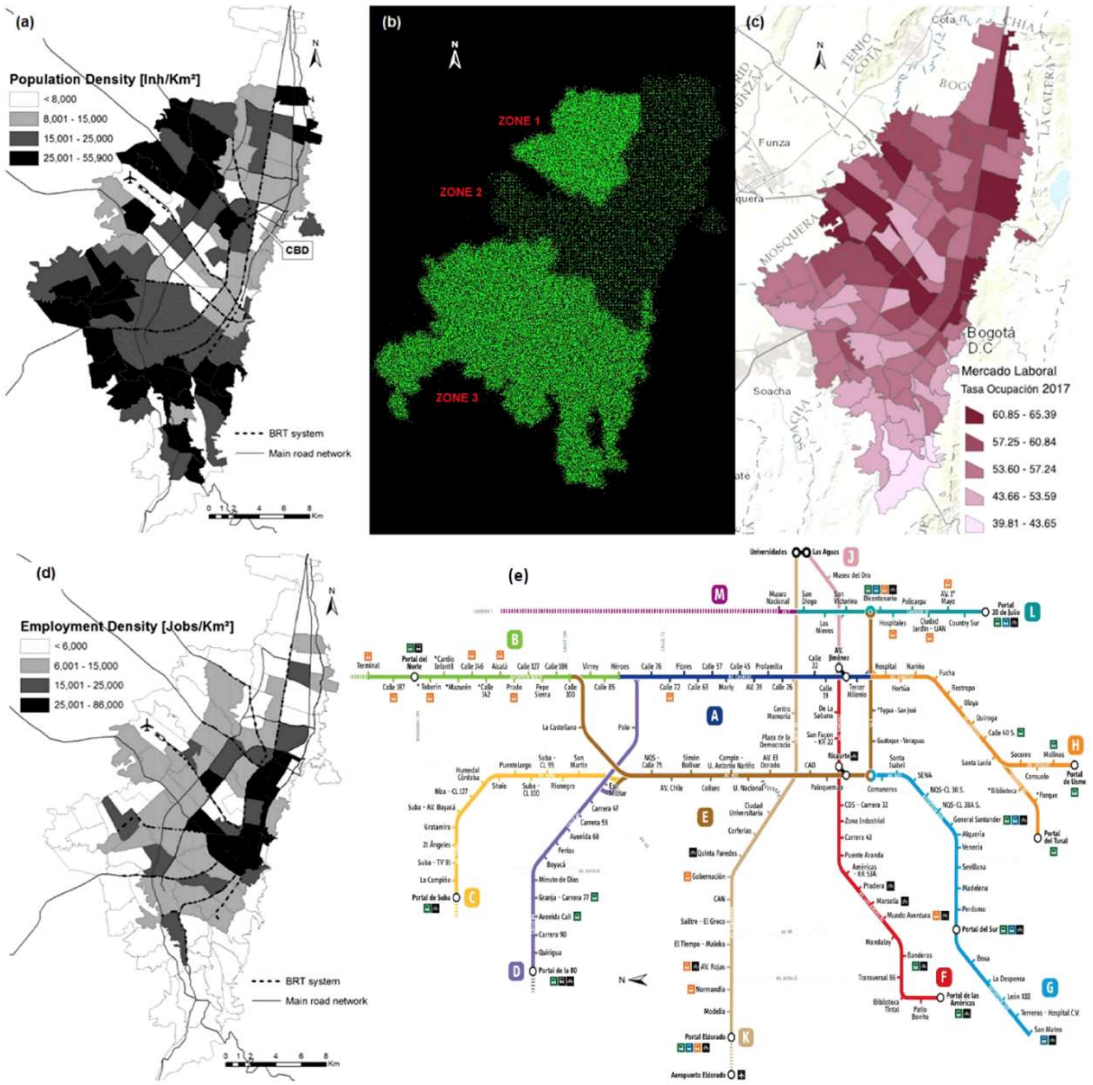

Figure 22. Population distribution in Bogotá (Guzman and Bocarejo 2017) (a), density distribution in the model (b), occupation distribution (Bogotá Planning Secretary 2011) (c), employment distribution (Guzman and Bocarejo 2017) (d), Bogotá bus network (e). For graphical reasons, the bus network is oriented with the north pointing left.

Because of the city socioeconomic structure, a large part of the population commutes every day from zones 1 and 2 to zone 3. Around 40% of commuters use the bus network (Figure 21e), which accounts for around 2.47 million daily trips (Transmilenio 2020). We use the technique described in Section 9, to model the bus network. Since we are interested in the flow from zones 1 and 3 to zone 2, we only account for routes A, B, C, D, F, G, H (Figure 21e). The number of people using each route and the time of the day when they use the bus is taken from statistics (Transmilenio 2020). Figure 23 shows the bus network in the model: the light dots represent the position of individuals that use the bus at a certain point of the day.

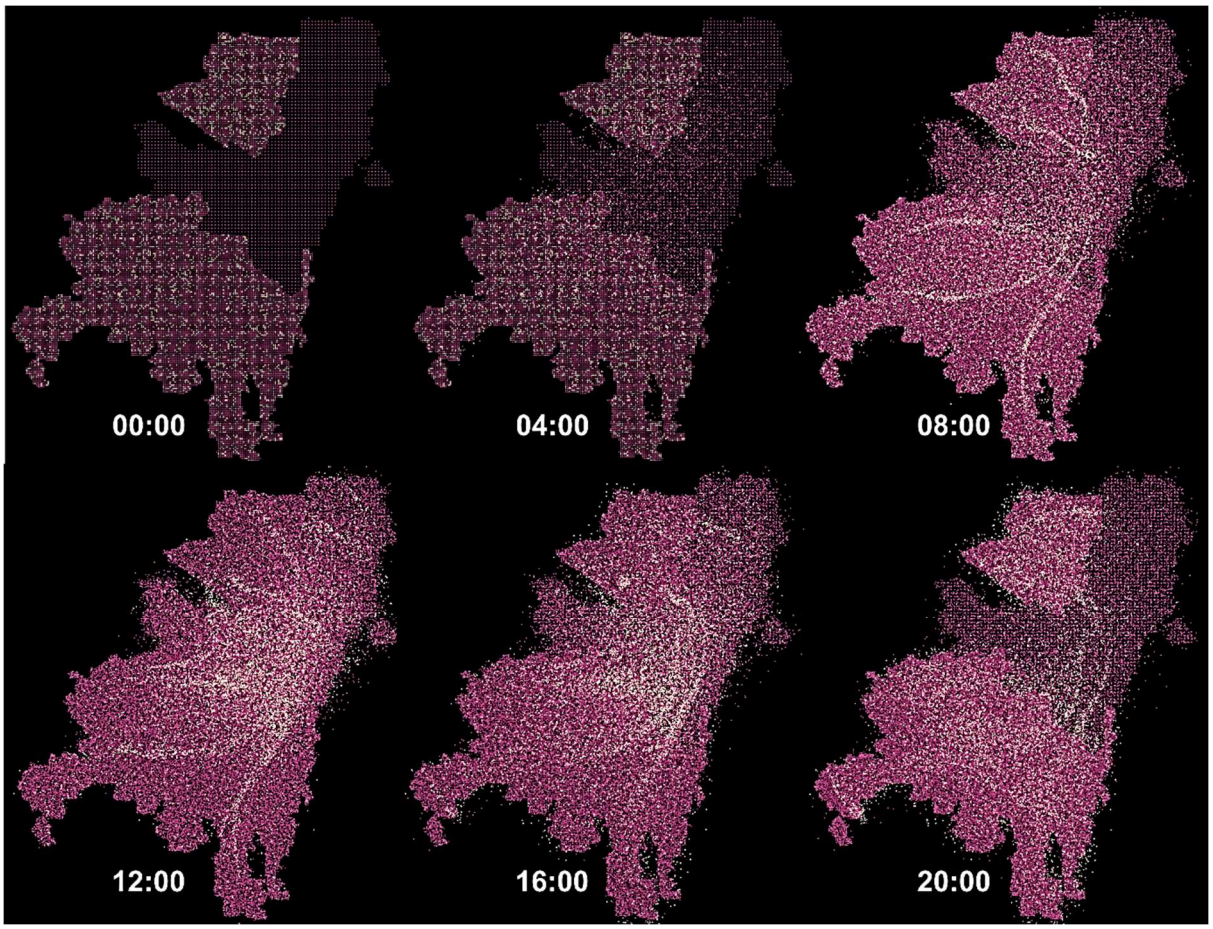

Figure 23. Instantaneous position of individuals taking the bus during the day (light particles) varying with time. For graphical reasons, only 1% of the population is shown.

The model is applied to the covid-19 infection in Bogotá. Simulations are carried out with LAMMPS on Athena Midlands+ HPC. Each simulation uses 16 Xeon E5-2680v4 processors with 28 cores each and takes around 80 hours. The value $p = 6 \cdot 10^{-4}\ \mathrm{min}^{-1}$ is derived from the pre-lockdown ('business as usual') real data; r and γ are considered a feature of the diseases and are the same for both Birmingham and Bogotá. Video 5 shows the evolution of the infection in Bogotá under the 'business as usual' scenario. Every frame of the video represents 6 hours: for graphical reasons, only 1% of the particles is shown. Figure 24 compares the model with real data. The lockdown was implemented on April 27th, 2020, the estimated number of people circulating during the lock-down was $5 \cdot 10^5$ (Estupiñán K. 2020), which is consistent with the data from the Google Mobility Report (Google 2000). According to the Mobility Report, the drop in mobility during the lockdown for retail and recreation was around 80% and around 70% for workplaces. Based on these data, we reduce the background mobility and the targeted mobility by the same amount. The bus network was closed and, therefore, not implemented in the lockdown model. On May 11th 2020, the lock-down was partially lifted and the estimated number of people circulating was $2.5 \cdot 10^6$ (Estupiñán K. 2020). The Google Mobility Report gives a reduction (with respect at the 'business as usual' scenario) of 59% for retail and recreation, 54% for workplaces. According to the bus operator (Transmilenio, 2020), the bus service was working at 35% of its capacity. Therefore, in the 'partial opening' model, we reduce the background mobility by 59%, the targeted mobility by 56% and the number of people using the bus by 65%.

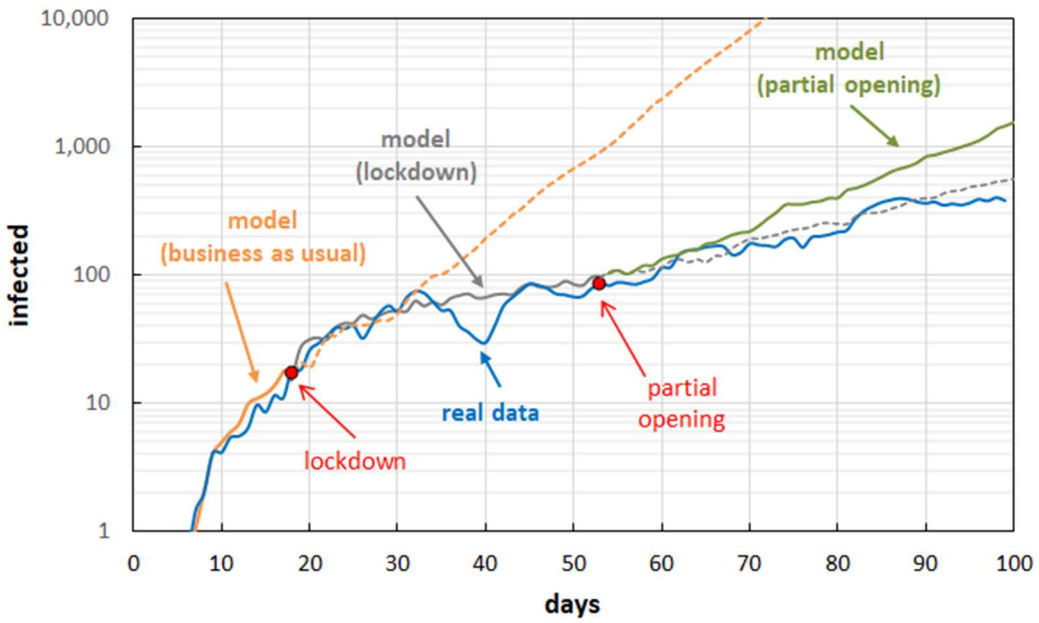

Figure 24. Comparison between real data (7 days moving average) and model output

The model works well for the 'business as usual' scenario, and the lockdown, but tends to overestimate contagion when simulating reopening after the lockdown. A possible explanation is that, after lockdown is lifted, people tend to be more careful about social distancing. Interestingly, the lockdown model works well also for the reopening, but it is just a fortuitous circumstance.

The model can assess various features of the city that influence people's mobility. Since the public transport system is considered one of the main sources of contagion in Bogotá, we can compare the 'business as usual' scenario with a 'no bus' scenario. All parameters of the two scenarios are the same, and the number of commuters in the two cases is also the same. The only difference is that, in the 'no bus' scenarios, commuters do not use the bust to move from home to the workplace. Figure 25 shows that, at the peak of infection, the two scenarios differ of ~4%, which correspond to ~320,000 people.

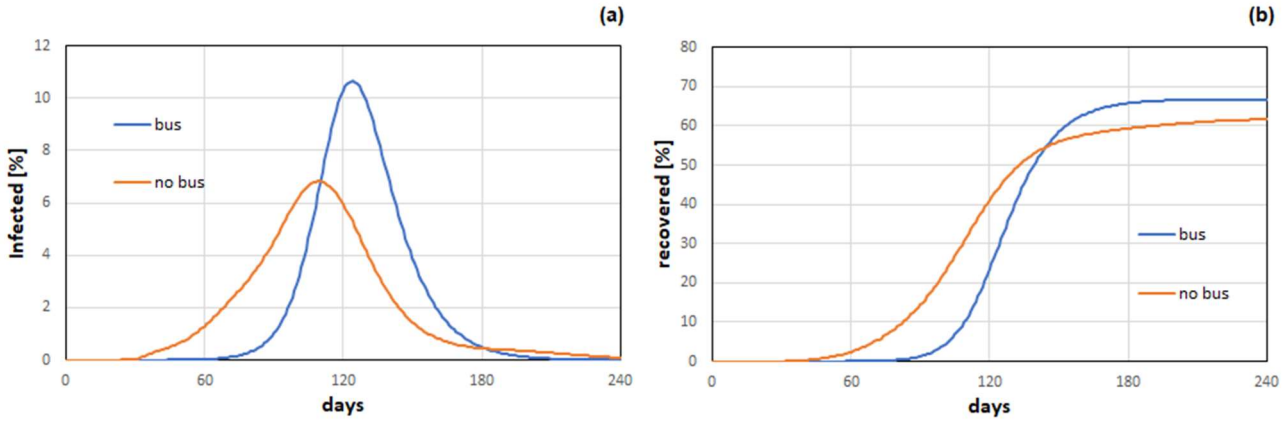

Figure 25. Time evolution of (a) infected and (b) recovered populations for Bogota comparing the 'business as usual' and the 'no bus' scenarios.

11. Conclusions

This study introduces Discrete Epidemiology: a modelling framework for simulating the spreading of infectious diseases within cities or countries. We generate digital copies of Birmingham in the UK and Bogotá in Colombia replicating their geography, infrastructure, and population. The daily activities of the virtual inhabitants and the spread of the disease are simulated for several months with a time resolution of 1 minute. Simulations accurately reproduce the covid-19 data for Birmingham and Bogotá both before and during the lockdown. By simulating the mobility, interaction, and potential for contagion of millions of digital individuals, our computer models are less reliant on data and have higher forecasting power than traditional epidemiological models. Except for one adjustable parameter calculable during the pandemic early stages, the model is derived from first principles, i.e. city's topography, population statistics and Google Mobility Reports. Our digital cities can be used as virtual labs for predicting the spread of infectious diseases in cities. This can provide policymakers with a new powerful tool for testing, predicting, and comparing the effects of policies aimed at containing epidemics before these policies are implemented.

Despite this, we believe Discrete Epidemiology has not achieved its full potential yet and can be improved in at least three directions. Firstly, the spatial fidelity to real-world topologies can be refined to account for the real location of every household, workplace, school, bus/train station, and other landmarks in the city. Secondly, several statistics and census data can be combined to derive more granular commuting patterns, which sometimes implies resolving inconsistencies in the available data (e.g. Fair at al. 2019). Finally, the numerical algorithm can be implemented on Graphics Processing Units (GPUs) to further increase its performance. Discrete Epidemiology's algorithm is derived from Molecular Dynamics, where atoms are replaced by individuals. Today, GPU-accelerated Molecular Dynamics simulations can handle billions, and even trillions, of atoms. In principle, our model could be scaled up to account for the entire human population. The proposed framework is not limited to Birmingham or Bogotá but can be adapted to any other city or region in the world. This would certainly require time and resources, but, it could occur within a modular framework where researchers around the world adapt Discrete Epidemiology to other cities and regions that are gradually interconnected to cover the entire planet.

12. Acknowledgement

This work was supported by the Engineering and Physical Sciences Research Council (EPSRC) grant number: EP/S019227/1. The authors would like to thank Prof Mikhail Prokopenko (Centre for Complex Systems, University of Sydney), Prof Philip Kuchel (School of Life and Environmental Sciences, University of Sydney) and Dr Lucy Gabriela Delgado (Public Health Laboratories Subdirectorate, Bogota's District Health Secretary) for their advice and comments. The computations described in this paper were performed using (a) University of Birmingham's BlueBEAR HPC service and (b) Athena at HPC Midlands+ (funded by the EPSRC on grant EP/P020232/1). The authors would also like to acknowledge the support with Athena of Dr Simon Branford at Birmingham's IT Research Group.

13. Nomenclature

β [s^{-1}]	contact frequency,
γ [s^{-1}]	recovery rate,
γ_f [s^{-1}]	friction coefficient in eq. (1),

ξ [kg m s^{-2}]	random force in eq. (1),
A [kg m^2 s^{-2}]	strength of the soft repulsive potential in eq. (6),
D [m^2 s^{-1}]	parameter in eq. (2),
f [-]	fraction of individuals with high mobility,
F_{REP} [kg m s^{-2}]	repulsion force in eq. (1) and eq. (7),
F_{DRIFT} [kg m s^{-2}]	drift force in eq. (1),
F_{EXT} [kg m s^{-2}]	external force in eq. (1),
g [-]	radial distribution function,
L [m]	reference length corresponding to 1 km in our simulation,
M [-]	instantaneous mobility defined in eq. (5),
<M> [-]	time-averaged mobility,
N_S [-]	initial susceptible population,
N_I [-]	initial infected population,
N_R [-]	initial removed population,
p [s^{-1}]	probability of infection of an individual within r for the duration of Δt,
r [m]	radius of infection,
r_p [m]	distance between particles in eq. (6),
r_c [m]	cut-off distance in eq. (6),
s [-]	fraction of individuals with high mobility wearing a mask,
t [s]	time,
T [s]	reference time corresponding to one day in our simulation,
v [m s^{-1}]	instantaneous particle velocity,
$<v>$ [m s^{-1}]	time-averaged particle velocity.

14. References

1. Alexiadis A., (2015) The Discrete Multi-Hybrid System for the simulation of solid-liquid flows PLoS ONE 10(5): e0124678
2. Ali S., Shah M. (2006) A Lagrangian particle dynamics approach for crowd flow segmentation and stability analysis *IEEE Conference on Computer Vision and Pattern Recognition* pp. 1–6.
3. Althoff, T., Sosič, R., Hicks, J., King, A., Delp, S. and Leskovec, J. (2017) Large-scale physical activity data reveal worldwide activity inequality *Nature* **547:**336-339.
4. Bela A.F., Wilkinson D. (2020) Technology intensity and homeworking in the UK, *Office for National Statistics* Available online: www.ons.gov.uk/employmentandlabourmarket/peopleinwork/employmentandemployeetypes/articles/technologyintensityandhomeworkingintheuk/2020-05-01 (last retrieved 10/05/20)
5. Bates A.G. (2015) Commuting to work, Changes to Travel to Work Areas: 2001 to 2011, *Office for National Statistics*. Available online: www.ons.gov.uk/employmentandlabourmarket/peopleinwork/employmentandemployeetypes/articles/commutingtoworkchangestotraveltoworkareas/2001to2011 (last retrieved 10/05/20)
6. Behera, S., Dogra, D.P., Bandyopadhyay, M.K., Royar, P.P. (2020) Understanding Crowd Flow Movements Using Active-Langevin Model, arXiv:2003.05626v2.
7. Birmingham City Council (2011) Birmingham Census 2011 report. Available online: https://researchbcc.files.wordpress.com/2012/09/census-2011-report-final.pdf (last retrieved 11/05/20)
8. Bogota's Planning Secretary (2011) Bogota's Working Age Population distribution; Occupation rate distribution Bogota: Bogota's Lord Mayoralty, Bogota's Planning Secretary. Available online:

http://sdpbogota.maps.arcgis.com/apps/View/index.html?appid=f98a94bcdca84c49ab03eda62b4ff0a1 (last retrieved 15/05/20)
9. Brienen NC, Timen A, Wallinga J, van Steenbergen JE, Teunis PF. (2010) The Effect of Mask Use on the Spread of Influenza During a Pandemic *Risk Analysis* **30**:1210-8
10. Cai, Q., Mitiche, A. and Aggarwal, J. K. (1995) Tracking human motion in an indoor environment," Proceedings., International Conference on Image Processing, Washington, DC, USA, pp. 215-218 vol.1, doi: 10.1109/ICIP.1995.529584.
11. Cliff O. M., Harding N., Piraveenan M., Erten E. Y., Gambhir M., Prokopenko M. (2018), Investigating Spatiotemporal Dynamics and Synchrony of Influenza Epidemics in Australia: An Agent-Based Modelling Approach *Simulation Modelling Practice and Theory* **87:**412-431
12. CDC - Centers for Disease Control and Prevention (2020) How to Protect Yourself & Others Available online: www.cdc.gov/coronavirus/2019-ncov/prevent-getting-sick/prevention.html (last retrieved 10/05/20)
13. Departamento Administrativo Nacional de Estadistica, Republica de Colombia (2017) Bogotá, D.C. (Capital District, Colombia) - Population Statistics, Charts, Map and Location available online at https://www.citypopulation.de/en/colombia/admin/11__bogot%C3%A1_d_c_/ (last retrieved 17/05/20)
14. Department of Transport (2014) Travel to school, *National Travel Survey 2014* Available online: https://assets.publishing.service.gov.uk/government/uploads/system/uploads/attachment_data/file/476635/travel-to-school.pdf (last retrieved 10/05/20)
15. Department of Transport (2019) Walking and cycling statistics, *National Statistics*. Available online: www.gov.uk/government/collections/walking-and-cycling-statistics (last retrieved 10/05/20)
16. Department of Transport (2018) West Midlands Road traffic statistics Available online: https://roadtraffic.dft.gov.uk/regions/10 (last retrieved 10/05/20)
17. Transmilenio (2020) Transmilenio en cifras febrero 2020 available online at https://www.transmilenio.gov.co/loader.php?lServicio=Tools2&lTipo=descargas&lFuncion=descargar&idFile=5778 last retrieved 14/06/20.
18. Einstein, A. (1905) Über die von der molekularkinetischen Theorie der Wärme geforderte Bewegung von in ruhenden Flüssigkeiten suspendierten Teilchen *Annalen der Physik* **322**: 549–560.
19. Estupiñán K. (2020) Bogotá empieza una nueva etapa de cuidado para enfrentar el COVID-19 available on-line https://bogota.gov.co/mi-ciudad/desarrollo-economico/cuarentena-medidas-para-la-reapertura-de-bogota-el-11-de-mayo-de-2020 last retrieved June 16, 2020
20. Fair K. M., Zachreson C., Prokopenko M. (2019) Creating a surrogate commuter network from Australian Bureau of Statistics census data, *Scientific Data* **6**:150.
21. Gallotti R., Louf R., Luck J., Barthelemy M. (2018) Tracking random walks *Journal of The Royal Society Interface* **15**:139
22. Gomez J., Prieto J., Leon E., Rodriguez A. (2020) INFEKTA: A General Agent-based Model for Transmission of Infectious Diseases: Studying the COVID-19 Propagation in Bogotá - Colombia medRxiv 2020.04.06.20056119
23. Google (2020) COVID-19 Community Mobility Reports available on-line at https://www.google.com/covid19/mobility/ (last retrieved 14/06/20)
24. Government Digital Service (2020) Coronavirus (COVID-19) in the UK Available online: https://coronavirus.data.gov.uk/ (last retrieved 21/05/20)
25. Grassberger, P. (1983) On the critical behavior of the general epidemic process and dynamical percolation *Mathematical Biosciences* **63**: 157–172
26. Guzman L. A., Oviedo D., Cardona R. (2006) Accessibility Changes: Analysis of the Integrated Public Transport System of Bogotá *Sustainability* **10**:3958.
27. Guzman, L. A., Bocarejo, J. P. (2017). Urban form and spatial urban equity in Bogota, Colombia. *Transportation research proceedings*, **25:**4491-4506

28. Kadau, K, Germann, T, Lomdahl, P (2006) Molecular dynamics comes of age: 320 billion atom simulation BlueGene/L. *International Journal of Modern Physics C* 17(12): 1755–1761.
29. Palmieri L, Andrianou X, Barbariol P, Bella A, Bellino S, Benelli E, et al. (2020). Characteristics of COVID-19 patients dying in Italy *Istituto Superiore di Sanità* Available online: https://www.epicentro.iss.it/coronavirus/bollettino/Report-COVID-2019_20_marzo_eng.pdf (last retrieved 10/05/20)
30. Park N. (2020) Population estimates for the UK, England and Wales, Scotland and Northern Ireland, provisional: mid-2019, *Office for National Statistics*. Available online: www.ons.gov.uk/peoplepopulationandcommunity/populationandmigration/populationestimates/bulletins/annualmidyearpopulationestimates/mid2019 (last retrieved 10/05/20)
31. Plimpton S. (1995) Fast Parallel Algorithms for Short-Range Molecular Dynamics *Journal Computational Physics*, **117**:1-19
32. OECD iLibrary (2018) Employment rate by age group available online: https://www.oecd-ilibrary.org/employment/employment-rate-by-age-group/indicator/english_084f32c7-en (last retrieved 17/05/20)
33. Rhee, I., Shin, M., Hong, S., Lee, K. (2011) On the Levy-Walk Nature of Human Mobility *IEEE/ACM Transactions on Networking* **19**:3.
34. Rubinstein, R.Y. (1991) Simulation and the Monte Carlo Method, John Wiley & Sons
35. Tchipev N., Seckler S., Heinen M., Vrabec J., Gratl F., Horsch M., Bernreuther M., Glass C.V., Niethammer C., Hammer N., Krischok B., Resch M., Kranzlmüller D., Hasse H., Bungartz H.J., Neumann P. (2019) TweTriS: Twenty trillion-atom simulation *International Journal of High Performance Computing Applications* **33**:838-854
36. UK Data Service (2011) Total and average distance travelled to place of work, *Office for National Statistics* Available online: www.statistics.digitalresources.jisc.ac.uk/dataset/total-and-average-distance-travelled-place-work-daytimeworkday-population-workplace-zones (last retrieved 10/05/20)
37. Watson, B. (2019) Employment in the UK: Estimates of employment, unemployment and economic inactivity for the UK, *Office for National Statistics* Available online: www.ons.gov.uk/employmentandlabourmarket/peopleinwork/employmentandemployeetypes/bulletins/employmentintheuk/october2019 (last retrieved 10/05/20)
38. West Midlands Combined Authority (2017) West Midlands travel trends 2017 Available online: https://www.tfwm.org.uk/media/2857/wm-travel-trends-2017.pdf (last retrieved 10/05/20)
39. Zachreson C., Fair K. M., Cliff O. M., Harding N., Piraveenan M., Prokopenko M. (2018) Urbanization affects peak timing, prevalence, and bimodality of influenza pandemics in Australia: Results of a census-calibrated model, *Science Advances*, **4:**eaau5294.